Learning-Based Tube MPC for Multi-Area Interconnected Power Systems with Wind Power and HESS: A Set Identification Strategy

Zhuoer An, Xinghua Liu, *Senior Member, IEEE,* Gaoxi Xiao, *Senior Member, IEEE,* Meng Zhang, *Senior Member, IEEE,* Zhongmei Pan, Yu Kang, *Senior Member, IEEE,* Nicholas Jenkins, *Fellow, IEEE*

***Abstract*—With the development of intelligent automation technology and advancement of modernization, the degree of interconnection between power systems is increasing. With the main purpose of involving hybrid energy storage systems (HESS) in optimizing system frequency, this work proposes a learning-based tube model predictive control (MPC) for the multi-area interconnected power systems with wind power and HESS. The suggested method has strong adaptability due to the introduction of a new robust constraint handled by a learning mechanism. By identifying the uncertainty set of coupling strength of online data in the learning stage, the optimal MPC problem is calculated in the adaptive stage, which effectively reduces the adverse effects of disturbances and noises in multi-area interconnected power systems. Moreover, an input to state stability criterion is provided to ensure the robust stability of the system with uncertain disturbances and noises. With simulations on a four-area interconnected power system with wind power and HESS, the effectiveness of proposed method is discussed on an improved IEEE 39-bus system.**

***Note to Practitioners*—To achieve a balance between load demand and power generation in multi-area interconnected power systems, various load frequency controls have been widely designed. The disturbances caused by high interconnectivity and the noise generated by electrical equipment pose a threat to the reliable operation of the power system. There is an urgent need to develop appropriate strategies to resist these interferences. So far, HESS have been widely applied in power systems with new energy to improve key system responses, such as power system frequency. This prompts defenders to design different types of external controllers to optimize the frequency deviation of the power system based on HESS. To tackle disturbances and noises which impose serious threat to system stability, we introduce a learning mechanism on the property of invariant sets and propose a learning-based tube MPC strategy that identifies disturbance invariant sets during the learning stage and calculates the optimal output during the adaptation stage. Moreover, simulations are presented to demonstrate that the proposed tube MPC strategy can provide satisfactory stability performance for interconnected power systems under disturbances and noises.**

Corresponding author: Xinghua Liu.

Z. An, X. Liu and Z. Pan are with the School of Electrical Engineering, Xi'an University of Technology, Xi'an 710048, China (e-mails: anzr@stu.xaut.edu.cn, liuxh@xaut.edu.cn, panpan@xaut.edu.cn).

G. Xiao is with the School of Electrical and Electronic Engineering, Nanyang Technological University, Singapore 639798, Singapore (e-mails: egxxiao@ntu.edu.sg).

M. Zhang is with the School of Cyber Science Engineering, Xi'an Jiaotong University, Xi'an 710049, China (e-mail: mengzhang2009@xjtu.edu.cn).

Y. Kang is with the Department of Automation, School of Information Science and Technology, University of Science and Technology of China, Hefei 230027, China (e-mail: kangduyu@ustc.edu.cn).

Nicholas Jenkins is with the School of Engineering, Cardiff University, Cardiff CF24 3AA, U.K. (e-mail: jenkinsn6@cardiff.ac.uk).

***Index Terms*—Multi-area interconnected power systems, learning-based tube model predictive control, load frequency control.**

I. Introduction

Multi-area interconnected power system can improve the efficiency, flexibility and expansibility of the traditional power system operation and management [1]–[3]. However, the multi-area interconnection makes the dynamic process of the whole power system more complicated, posing a challenge to the stable operation of the power system. The frequency of power system is the key index for evaluating power quality. During periods with unbalanced power generation and load demand caused by load changes, frequency deviation from the rated value may occur, which greatly threatens system stability. To track the random changes of load disturbances, it is necessary to control the output power of the generator set in real time. The load frequency control (LFC) therefore becomes an important method to ensure the power supply quality and reliable operation of the power system under a high degree of interconnection [4]–[6].

The frequency oscillations caused by the large-scale and complex interconnected power systems are more severe than those often faced by the single grid [7], [8]. Many strategies have been proposed to ameliorate the frequency stability of multi-area power systems [9]–[11]. Li et al. [12] addressed the LFC problem for the semi-Markov jump interconnected power systems suffering from actuator failures and incomplete transition rates. For multi-area power systems under the false data injection attacks, an indirect–direct secure strategy was proposed for the LFC problem [13]. An LFC controller based on the T–S fuzzy model was proposed to effectively solve the frequency problem of the interconnection line in the interconnected power system with wind power grid [14]. To address the LFC problem in multi-area power systems under actuator failures, an LFC control scheme was proposed which considered the communication bandwidth constraints and uncertainties [15].

Model predictive control (MPC) not only has the advantage of robust control in solving system parameter uncertainty, but also has the ability to use predictive control to handle system constraints [16]–[18]. In [19], a robust multivariable MPC was proposed for the solution of LFC in a multi-area power system based on the multivariable LFC characteristic, generation rate constraint and uncertainty. Tube MPC separates the nominal states from the actual states and transforms the control of the actual system into the nominal system. Therefore, this MPC strategy can adjust the system control performance by designing constraint sets flexibly, and has strong robustness in practical engineering applications. In [20], a decentralized controller for improving the transient stability of multimachine power systems was proposed. A thermal management system model with uncertain parameters for the fuel cell system to simulate unforeseeable disturbances in real systems was developed based on tube MPC in [21]. Similarly, Literature [22] studied a frequency regulation method with MPC applied to a renewable penetrated isolated grid in the presence of a large number of electric vehicles. In addition, tube MPC controllers capable of resisting the external disturbance were designed in [23] and [24] to efficiently regulate the frequency of the power system. However, traditional roubust MPC does not have the parameter adaptivity and cannot update the control parameters in real time in response to the change of environment, which means that control performance and system stability may face challenges in complex power systems.

To make the multi-area interconnected power system more intelligent while ensuring the safety and reliability of power transmission, the frequency modulation strategy with learning awareness is worth considering. In [25], an LFC strategy based on learning MPC was proposed for multi-microgrids in the vehicle networks. In [26], the policy learning problem was proposed for the nonlinear MPC with system constraints, where the nonlinear MPC policy was learned offline. Tang et al. [27] investigated an adaptive MPC strategy for LFC of hybrid power system. However, most adaptive strategies still only consider a single interference after significantly increasing complexity, which cannot achieve satisfactory frequency regulation performance.

In multi-area interconnected power systems, hybrid energy storage systems (HESS) is mainly responsible for generating and absorbing active power from the power systems to smooth out fluctuations in system frequency. In view of the negative effects of random fluctuations of wind power on the power grid, literature [28] proposed a wind power filtering method to appropriately adjust the HESS size using a wavelet capacity allocation algorithm. In [29], a model on peak load shifting was proposed for a power system with energy storage device and wind power based on the situation awareness theory. Moreover, a dynamic and unified power management method was designed in [30] for a wind-photovoltaic powered low-voltage direct current microgrid equipped with an actively configured HESS unit. Currently, HESS is more applied in the electric vehicles, auxiliary new energy power generation systems, photovoltaic power generation systems and other fields [31]–[33].

In this work, our goal is to design a learning-based tube MPC strategy to ensure the stability of interconnected power systems under disturbance and noise. Based on the uncertain interference data learned from each region, the proposed controller coordinates HESS by updating the invariant set and control signal to quickly restore the system frequency to the expected value. The main contribution of this work are highlighted as

1) To reduce the adverse effects of new energy participating in the LFC problem in multi-area power systems, a four-area interconnection structure with HESS is constructed to improve the frequency regulation capability.
2) Unlike previous studies [34]–[36], the proposed strategy calculates the optimal predicted state and input in the adaptive stage by identifying the uncertainty set of the coupling strength of the state during the learning stage, improving system robustness and ensuring its frequency stability under disturbance and noise.
3) By constructing updateable invariant sets, a reliable condition for multi-area power systems with wind power and HESS under the learning-based tube MPC method to be stable is derived, and its excellence is demonstrated through simulations.

The work is constructed as follows. Section II introduces the wind power system, model of LFC, tube control strategy and the proposed learning-based tube MPC strategy. Section III discusses the details of the learning and adaptation stages of the proposed strategy, and derives the stability conditions for applying this strategy to participate in the LFC problem in multi-area interconnected power systems under disturbances and noises conditions. Section IV discusses the power systems performance of the proposed method through simulations. In the end, section V concludes our work.

Notation. $\oplus$ represents the Minkowski sum and is defined by $A \oplus B \triangleq \{a+b \mid a \in A, b \in B\}$. $\ominus$ represents the Minkowski difference and is defined $A \ominus B \triangleq \{a \mid a \oplus B \subseteq A\}$. Moreover, we use $[\cdot]\, j$ and $|\cdot|j$ to represent the diagonal element in the j-th row of a matrix and the summation of the absolute values of the entries in the j-th row of a matrix, respectively.

II. Preliminary work

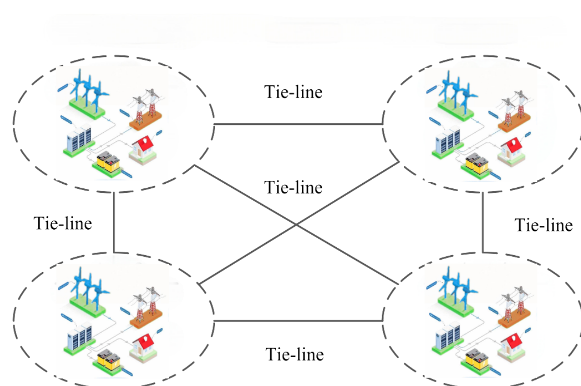

Fig. 1. Structure of four-area power system with wind power and HESS.

This work takes a four-area interconnected power system as a case study to explore the frequency regulation problem of multi-area interconnected systems with wind power and HESS, where power transmission between areas is based on tie lines. Figure 1 illustrates the structure of the considered power system, where each area includes a generator seystem, a user load, a wind power system representing new energy, and a HESS.

A. Wind Power System

The wind power generator can be described by a few parameters. Below we introduce these parameters and discuss on the relations between them. The relation between output power P_{wpi} of the windmill and some of its main parameters can be presented as

$$P_{wpi} = \frac{C_{wi}(\lambda, \beta) V_{wi}^3 \rho A_{wi}}{2} \tag{1}$$

where V_{wi} is the wind speed, ρ and A_{wi} are the air density and rotor cross-section, respectively, $C_{wi}(\lambda, \beta)$ is defined as the power coefficient, $\lambda = R\varpi / V_{wi}$ is the tip speed ratio, β is the pitch angle, R is radius of a windmill, ϖ is the speed of rotor angular.

Due to the fact that the inertia of the wind turbine is much greater than that of the generator when connected to it, the transient process of the generator is ignored, and the output power of wind power can be described as

$$P_{wi} = \frac{-3V_P^2 \partial (1+\partial) R_2}{(R_2 - \partial R_1)^2 + (\partial X_1 + \partial X_2)^2} \tag{2}$$

where V_P is the phase voltage, $\partial = (\varpi_0 - \varpi)/\varpi_0$ is the slip of generator, R_1 and R_2 are the stator resistance and rotor resistance, and X_1 and X_2 are the stator reactance and rotor reactance, respectively.

B. Model of Load Frequency Control

The major objective of the LFC problem in a multi-area power system is to ensure that the frequency deviation of each control area tends to zero, and its modified model is shown in Fig. 2. LFC of the four-area power system takes area control error (ACE) as feedback variable to ensure the aforementioned objective. The ACE of the Area-i is

$$ACE_i = \Delta P_{tie,i} + \frac{\beta_i}{T_{R_i}} \Delta f_i \tag{3}$$

where $\Delta P_{tie,i}$ is the interchanged power of tie-line, Δf_i is the frequency deviation, β_i is the frequency deviation setting, and T_{Ri} is the speed regulation gain.

The state space model of the power system in Area-i is

$$\begin{cases} \dot{x}_i = A_i x_i + B_i u_i + w_i + d_i \\ y_i = C_i x_i \end{cases} \tag{4}$$

where $x_i = \begin{bmatrix} \Delta f_i & \Delta P_{m_i} & \Delta P_{v_i} & \Delta P_{tie,i} & \int y_i \end{bmatrix}^{\mathrm{T}}$ is the state variable for the Area-i, $u_i = P_{ci}$ is the input variable, and $y_i = ACE_i$ is the output variable. w_i and d_i are disturbances and noises. The physical significance of system parameters are given in Table I. A_i, B_i and C_i represent the appropriate matrices for power systems.

$$A_i = \begin{bmatrix} \frac{-D_i}{T_{m_i}} & \frac{1}{T_{m_j}} & 0 & \frac{-1}{T_{m_i}} & 0 \\ 0 & \frac{-1}{T_{d_i}} & \frac{1}{T_{d_j}} & 0 & 0 \\ \frac{-1}{T_{R_i} T_{g_i}} & 0 & \frac{-1}{T_{g_i}} & 0 & 0 \\ \sum_{j=1, j\neq i}^{N} 2\pi T_{ij} & 0 & 0 & 0 & 0 \\ \beta_i & 0 & 0 & 1 & 0 \end{bmatrix},$$

$$B_i = \begin{bmatrix} 0 & 0 & -\frac{1}{T_{gi}} & 0 & 0 \end{bmatrix}^{\mathrm{T}},$$

$$C_i = \begin{bmatrix} \beta_i & 0 & 0 & 1 & 0 \\ 0 & 0 & 0 & 0 & 1 \end{bmatrix}^{\mathrm{T}}$$

TABLE I
PARAMETER METRICS

Parameters	Physical significance
ΔP_{vi}	deviation of turbine valve position
ΔP_{mi}	deviation of generator mechanical power
ΔP_{di}	load disturbance
ΔP_{wi}	the wind power deviation
Δf_i	frequency deviation
P_{ci}	the power delivered by HESS to control area
T_{mi}	time constant of power system
T_{di}	time constant of generator
T_{gi}	time constant of governor
T_{ij}	interconnection constant between the areas
D_i	equivalent damping coefficient of generator

The LFC model of the multi-area power systems can be described as

$$\begin{cases} x_i(t+1) = A_i x_i(t) + B_i u_i(t) + w_i(t) + d_i(t) \\ y_i(t) = C_i x_i(t) \end{cases} \tag{5}$$

where the disturbances $w_i(t) = \sum_{j\in\mathcal{N}_i^-} a_{ij}(t) E_j x_j(t) \in \mathcal{W}_i$, and the noise vector $d_i(t)$ is assumed to be located in a known set $\mathcal{D}_i = \{d_i(t) : \Xi_i d_i(t) \leq 1\}$ which includes the origin in its interior. $a_{ij}(t)$ is the coupling strength that satisfies $0 \leq a_{ij}^{\min}(t) \leq a_{ij}(t) \leq a_{ij}^{\max}(t)$, where the bounds $a_{ij}^{\min}(t)$ and $a_{ij}^{\max}(t)$ are known. $x_i(t) \in \mathcal{X}_i$ and $u_i(t) \in \mathcal{U}_i$ are state constraints and control constraints, respectively.

Remark 1. *The interconnected systems with the uncertain coupling (5) are suitable for large-scale complex systems, including microgrids and power systems. In this work, $d_i(t)$ is the noise caused by electrical equipment in the power system, which is a disturbance term different from $w_i(t)$.*

Remark 2. *A four-area interconnected system expands the physical coverage and node density of the grid through additional interconnections, forming a more robust tie-line network. In this work, our interconnected structure enhances frequency regulation through multi-area coordination and multi-technology synergy. Compared with the traditional four-area structure, its core improvement lies in strengthening power support and inertial response through redundant inter-connection, and adopting HESS to achieve full-time frequency support to improve system frequency stability.*

C. Tube MPC strategy

Within the tube MPC framework, the actual system's state path consistently stays within an invariant set that is centered around the nominal system's state path, as shown in Fig. 3. Consequently, as the nominal system converges towards the origin, the actual system is similarly restricted to a vicinity

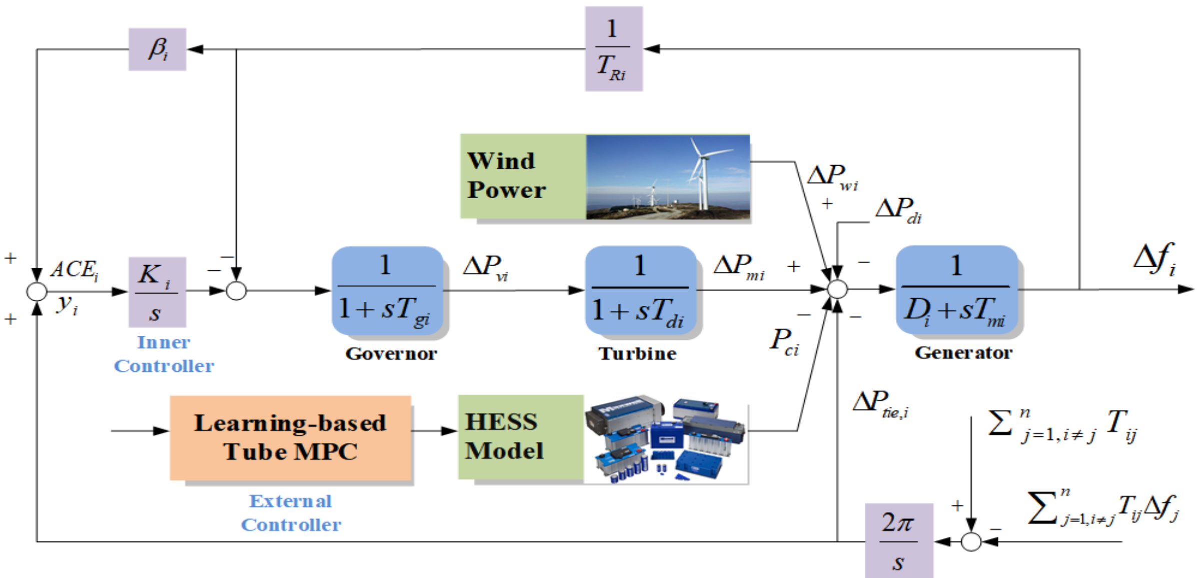

Fig. 2. Structure of Area-i in interconnected power systems.

close to the origin, which ensures the asymptotic stability of the actual control system.

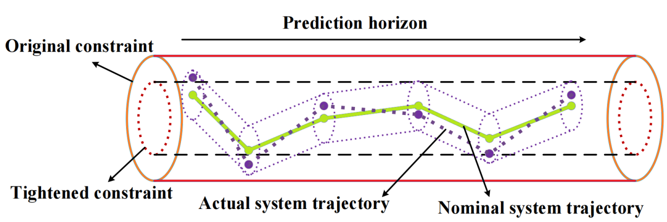

Fig. 3. Conceptual diagram of tube control strategy.

The nominal system can be defined as

$$\bar{x}_i(t+1) = A_i\bar{x}_i(t) + B_i\bar{u}_i(t) \tag{6}$$

where $\bar{x}_i(t) \in \bar{\mathcal{X}}_i$, $\bar{u}_i(t) \in \bar{\mathcal{U}}_i$.

To reduce the impact of disturbances and lead the nominal states to be closer to the actual states, the system control law $u_i(t) = \bar{u}_i(t) + K_i(x_i(t) - \bar{x}_i(t))$ is designed, where feedback control gain K_i is chosen such that $A_{Ki} = A_i + B_iK_i$ is stable. In addition, to better illustrate the relationship between the actual states and the nominal states under constraints, we introduce the error dynamics as

$$e_i(t+1) = A_{Ki}e_i(t) + w_i(t) + d_i(t) \tag{7}$$

where $e_i(t) = x_i(t) - \bar{x}_i(t)$.

A better setting of constraint of errors can lead to stronger control effects. To facilitate the subsequent design of the tube MPC method, we deal with state and control constraints based on the properties of robust invariant set (RIS), which is defined as follows.

Definition 1. *[24] A set $\mathcal{Z}_i$ is robustly positively invariant under $x_i(t+1) = Ax_i(t) + Bu_i(t)$, $u_i(t) = K_ix_i(t)$, and $x_i(t) \in \mathcal{X}_i$, $u_i(t) \in \mathcal{U}_i$, if $x_i(t+1) \in \mathcal{X}_k$, $x_i(t) \in \mathcal{X}_i$, $u_i(t) \in \mathcal{U}_i$ for all $x_i(t) \in \mathcal{X}_k$.*

Based on **Definition 1**, the following MPC problem can be obtained as

$$\begin{aligned} &\min J_i \\ &\text{s.t.} \\ &\begin{cases} x_i(t) - \bar{x}_i(0 \mid t) \in \mathcal{Z}_i \\ \bar{x}_i(k+1 \mid t) = A_i\bar{x}_i(k \mid t) + B_i\bar{u}_i(k \mid t), k \in \mathbb{N}_{[0,N-1]} \\ \bar{x}_i(k \mid t) \in \bar{\mathcal{X}}_i, k \in \mathbb{N}_{[0,N-1]} \\ \bar{u}_i(k \mid t) \in \bar{\mathcal{U}}_i, k \in \mathbb{N}_{[0,N-1]} \\ \bar{x}_i(N \mid t) \in \xi\bar{\mathcal{X}}_i, \xi \in (0,1) \end{cases} \end{aligned} \tag{8}$$

where $\mathcal{Z}_i$ is an RIS with the interferences $w_i(t)$ and $d_i(t)$. $\xi \in (0,1)$ is a constraint parameter that adjusts the position of the nominal state within the constraint set. $\bar{\mathcal{X}}_i$ and $\bar{\mathcal{U}}_i$ are tightened constraint sets. $\bar{x}_i(N \mid t) \in \xi\bar{\mathcal{X}}_i$ represents that the system can reach an invariant set of terminals that satisfy state and input constraints.

Remark 3. *In this work, we treat the coupling term as an interference with the conservative properties, which leads to a decentralized optimal control problem rather than a distributed optimal control problem. However, for systems with fast dynamics, decentralized optimal control problems require less communication.*

Remark 4. *Accurate models for the new subsystems can be determined before they are integrated, but the coupling strength of their interaction with the network can only be assessed during online operation after their connection.*

D. Learning-based tube MPC strategy

The learning stage of learning uncertainty and adaptation stage of calculating the optimal control action at each moment constitute the proposed learning-based tube MPC method. In this work, we assume that each subsystem can interact with its neighbors at each moment and neighbors only need to communicate once at each moment during the learning stage.

In the learning stage, our goal is to minimize the size of the uncertainty set $\mathcal{W}_i$ by learning the bounds $a_{ij}^{\min}(t)$ and $a_{ij}^{\max}(t)$ of the $a_{ij}(t)$ as more data is gathered online. Therefore, the set $\mathcal{W}_i$ is updated based on $a_{ij}(t)$, and determining a smaller upper bounds can help accelerate its size reduction. In the adaptation stage, our goal is to adjust MPC in a timely manner based on the learned $\mathcal{W}_i$. In addition, the calculation of local optimal control inputs based on updated $\mathcal{W}_i$ also needs to be considered. Moreover, the adapted MPC ingredients contain RIS $\mathcal{Z}_i$, control gain K_i, state constraint set $\bar{\mathcal{X}}_i$ and input constraint set $\bar{\mathcal{U}}_i$. The subsequent learning strategy design for identifying sets is mainly based on these ingredients.

The required constraints for updating are

$$\bar{\mathcal{X}}_i(t) \oplus \mathcal{Z}_i(t) \subseteq \mathcal{X}_i \tag{9}$$

$$\bar{\mathcal{U}}_i(t) \oplus K_i(t)\mathcal{Z}_i(t) \subseteq \mathcal{U}_i \tag{10}$$

To maintain the convexity of the optimal problem during the adaptation stage, additional constraints are incorporated to ensure satisfying the aforementioned conditions.

Remark 5. *The designed MPC ingredients and uncertainty sets are functions of the time because these ingredients are updated at the moment t according to the learned uncertainty sets $\mathcal{W}_i(t)$, which are functions of coupling strengths $a_{ij}^{\min}(t)$ and $a_{ij}^{\max}(t)$ at that time.*

III. Main Results

A. Learning-based tube MPC method design

This section introduces the proposed tube MPC method by exploring the identification of set members for uncertain sets in online learning during the learning stage. Following this, we derive the constraints that are incorporated into each subsystem's local online optimal control problem during the adaptation stage. Hence, our goal is to optimize and constrain the proposed tube MPC method based on the learning stage and adaptation stage.

Firstly, we define the learning stage to ensure that the uncertainty set $\mathcal{W}_i(t)$ can be learned in real-time as more online data is obtained. Obviously, this set is influenced by uncertain boundaries and can be more accurately represented by refining these boundaries.

Assuming that at the moment t-1, the bounds of uncertain parameters $a_{ij}(t)$ are $a_{ij}^{\min}(t-1)$ and $a_{ij}^{\max}(t-1)$, respectively. To enhance these bounds' estimates at the moment $t-1$, the feasible parameter set with inequality for each $a_{ij}(t)$ is

$$F_{ij}a_{ij}(t) \leq f_{ij}(t-1) \tag{11}$$

where subvectors $f_{ij}(t-1) = \left[a_{ij}^{\max}(t-1) \;\; -a_{ij}^{\min}(t-1)\right]^T$, matrices $F_{ij} = \left[\begin{array}{cc} 1 & -1 \end{array}\right]^T$.

By defining θ_i that includes the entire uncertain data to be learned for the subsystem, we have

$$F_i\theta_i \leq f_i(t-1) \tag{12}$$

where F_i is a block diagonal matrix with F_{ij}, f_i is a vector vertically concatenating f_{ij}.

Then, by defining $\varepsilon_i(t-1)$ to be a matrix horizontally concatenating vectors $E_jx_j(t-1)$, $\Omega_i(t-1) = -\Xi_i\varepsilon_i(t-1)$ and $\omega_i(t-1) = 1 + \Xi_iA_ix_i(t-1) + \Xi_iB_iu_i(t-1) - \Xi_ix_i(t)$, we can construct the parameter set such as

$$\Theta_i = \{\theta_i : \Omega_i(t-1)\theta_i \leq \omega_i(t-1)\} \tag{13}$$

Obviously, these bounds that determine the control strength are updated with the calculation of each optimization problem. To obtain the optimal control trajectory during the adaptation stage, the lower and upper limits of $a_{ij}(t)$ are designed as

$$\begin{aligned} &-a_{ij}^{\min}(t) = \min e_{ij}^T(t)\theta_i, a_{ij}^{\max}(t) = \max e_{ij}^T(t)\theta_i \\ &\text{s.t.} \left[\begin{array}{c} F_i \\ \Omega_i(t-1) \end{array}\right]\theta_i \leq \left[\begin{array}{c} f_i(t-1) \\ \omega_i(t-1) \end{array}\right] \end{aligned} \tag{14}$$

where $e_{ij}(t)$ is a unit vector.

In this work, the uncertainty set $\mathcal{W}_i(t)$ in (5) is learned by solving the problem (14) that identifies uncertain parameter boundaries, which are communicated through data between neighbors during the adaptation stage.

Remark 6. *The goal of this stage is to find the maximum and minimum values of the parameters within the feasible sets. Based on (12) and (13), $-a_{ij}^{\min}(t) \leq a_{ij}(t) \leq a_{ij}^{\max}(t)$ for all $t \geq 0$ if $-a_{ij}^{\min}(t)$ and $a_{ij}^{\max}(t)$ are calculated by (14) and $-a_{ij}^{\min}(0) \leq a_{ij}(0) \leq a_{ij}^{\max}(0)$. Therefore, it is guaranteed that $-a_{ij}^{\min}(t) \geq -a_{ij}^{\min}(t-1)$ since $-a_{ij}^{\min}(t)$ is obtained by minimizing the whole possible values satisfying $a_{ij}(t) \geq -a_{ij}^{\min}(t-1)$. Similarly, based on considerations of the upper bounds, we can derive that $\mathcal{W}_i(t) \subseteq \mathcal{W}_i(t-1)$ for all t, which indicates that there is no risk of having an expanding size of the uncertainty set $\mathcal{W}_i(t)$.*

Secondly, we define the adaptation stage with the objective of solving online optimal control problems based on the learned set $\mathcal{W}_i(t)$. To adjust MPC online and ensure that robust constraints are met, (9) and (10) should be satisfied.

Based on **Definition 1**, we can obtain that set $\mathcal{Z}_i(t)$ is a robustly invariant within the considered uncertainty sets and dynamics by assuming that $\mathcal{Z}_i(t) = \left\{e_i : e_i^TZ_ie_i \leq \alpha_i^2(t)\right\}$ if $\|e_i(t+1)\|_{Z_i}^2 \leq \alpha_i^2(t)$ for all e_i satisfying $\|e_i\|_{Z_i}^2 \leq \alpha_i^2(t)$, $\left\|w_{ij}(t) - a_{ij}^{\max}(t)\right\| \leq a_{ij}^{\max^2}(t)$ and $\|d_i(t)\|_{\Xi_i}^2 \leq 1$. We define tightened state and control sets as $\bar{\mathcal{X}}_i(t) = \{\bar{x}_i : G_i\bar{x}_i \leq g_i(t)\}$ and $\bar{\mathcal{U}}_i(t) = \{\bar{u}_i : H_ix_i \leq h_i(t)\}$, respectively. $\alpha_i(t)$, $g_i(t)$ and $h_i(t)$ are viewed as decision variables in the proposed strategy to update the MPC ingredients.

Assuming that $G_i^{(j)}$ and $H_i^{(j)}$ are the j-th row of the matrices G_i and H_i, respectively. The Minkowski sum of $\bar{\mathcal{X}}_i(t)$ and $\bar{\mathcal{Z}}_i(t)$ is involved in set $\mathcal{X}_i$ if for all $j \in \{1, \ldots, q_i\}$, we can deduce that $G_i^{(j)}\left(\bar{x}_{e_i} + \bar{x}_{s_i}\right) \leq 1$ for all $\bar{x}_{e_i}$ such that $\|\bar{x}_{e_i}\|_{Z_i}^2 \leq \alpha_i^2(t)$ and for all $\bar{x}_{s_i}$ such that $G_i\bar{x}_{s_i} \leq g_i(t)$, respectively. The above analysis is to ensure that all states in the state constraint set can always maintain finite offset through $\bar{\mathcal{Z}}_i(t)$.

For further analysis, defining $\alpha_i(t)s_i = \bar{x}_{e_i}$ and $g_i(t)r_i = \bar{x}_{s_i}$ yields

$$G_i^{(j)}\alpha_i(t)s_i + G_i^{(j)}g_i(t)r_i \leq 1 \tag{15}$$

where $s_i^T Z_i s_i \leq 1$, $G_i r_i \leq 1$ and $j \in \{1, \ldots, q_i\}$.

Based on S-lemma [37], this condition is given by

$$\left[\begin{array}{cc} \mu_{ij}(t) Z_i & -0.5 {G_i^{(j)}}^T \alpha_i(t) \\ * & 1-\mu_{ij}(t)-g_i(t) \end{array}\right] \geq 0 \tag{16}$$

where $\mu_{ij}(t) > 0$ for all $j \in \{1, \ldots, q_i\}$.

Inspired by [38], we assume $M_i(t)$ and $\lambda_{ij}(t) > 0$ such that $M_i(t) \leq \lambda_{ij}(t) \kappa_i^{-1} (\kappa_i = K_i(t) \alpha_i(t) Z_i^{-1} \alpha_i(t) K_i^T(t))$ for all $j \in \{1, \ldots, p_i\}$. The Minkowski sum of $\bar{\mathcal{U}}_i(t)$ and $K_i(t) \bar{\mathcal{Z}}_i(t)$ is involved in set $\mathcal{U}_i$ if for all $j \in \{1, \ldots, p_i\}$, so there are $H_i^{(j)} (\bar{u}_{e_i} + \bar{u}_{s_i}) \leq 1$ for all $\bar{u}_{e_i}$ such that $\|\bar{u}_{e_i}\|^2_{\kappa_i^{-1}} \leq \alpha_i^2(t)$ and for all $\bar{u}_{s_i}$ such that $H_i \bar{u}_{s_i} \leq h_i(t)$, respectively.

By defining $s_i = \bar{u}_{e_i}$ and $h_i(t) r_i = \bar{u}_{s_i}$, we have

$$H_i^{(j)} s_i + H_i^{(j)} h_i(t) r_i \leq 1 \tag{17}$$

where $s_i^T \kappa_i^{-1} s_i \leq 1$, $H_i r_i \leq 1$ and $j \in \{1, \ldots, p_i\}$.

Based on Schur Complement and S-lemma, this condition is given by

$$\begin{gathered} \left[\begin{array}{cc} M_i^{-1}(t) & K_i(t)^T \alpha_i(t) \\ * & \lambda_{ij}(t) Z_i \end{array}\right] \geq 0, \\ \left[\begin{array}{cc} M_i^{-1}(t) & 0.5 M_i^{-1}(t) {H_i^{(j)}}^T \\ * & 1-\lambda_{ij}(t)-h_i(t) \end{array}\right] \geq 0 \end{gathered} \tag{18}$$

Furthermore, the new MPC problem can be obtained as

$$\begin{aligned} & \min J_i \\ & \text{ s.t. } \\ & \left\{\begin{array}{l} x_i(t)-\bar{x}_i(0 \mid t) \in \mathcal{Z}_i(t) \\ \bar{x}_i(k+1 \mid t)=A_i \bar{x}_i(k \mid t)+B_i \bar{u}_i(k \mid t), k \in \mathbb{N}_{[0, N-1]} \\ \bar{x}_i(k \mid t) \in \bar{\mathcal{X}}_i(t), k \in \mathbb{N}_{[0, N-1]} \\ \bar{u}_i(k \mid t) \in \bar{\mathcal{U}}_i(t), k \in \mathbb{N}_{[0, N-1]} \\ \bar{x}_i(N \mid t) \in \xi \bar{\mathcal{X}}_i(t), \xi \in(0,1) \\ (16), \mu_{ij}(t) \geq 0, j \in\{1, \ldots, q_i\} \\ (18), \lambda_{ij}(t)>0, j \in\{1, \ldots, p_i\} \end{array}\right. \end{aligned} \tag{19}$$

The decision variables are $\bar{x}_i(k \mid t)$, $\bar{u}_i(k \mid t)$, $\alpha_i(t)$, $g_i(t)$, $h_i(t)$, $\mu_{ij}(t)$ for all $j \in \{1, \ldots, q_i\}$ and $\lambda_{ij}(t)$ for all $j \in \{1, \ldots, p_i\}$, which are used to update the nominal state and invariant set. To ensure robust constraint satisfaction, (19) is solved based on (8) and $u_i(t) = \bar{u}_i(t) + K_i(x_i(t) - \bar{x}_i(t))$.

According to $u_i(t) = \bar{u}_i(t) + K_i(x_i(t) - \bar{x}_i(t))$ and (5), we can obtain that

$$\begin{aligned} x_i^*(t+1) = & A_i x_i^*(t) + B_i \bar{u}_i^*(t) + B_i K_i^*(t)\left(x_i^*(t) - \bar{x}_i^*(t)\right) \\ & + A_g E_i x_i^*(t) + d_i(t) \end{aligned} \tag{20}$$

where A_g is the adjacency matrix and * is the optimal solution.

Then, by defining $e_i^*(t) = x_i^*(t) - \bar{x}_i^*(t)$ we have

$$e_i^*(t+1) = A_{Ki}^*(t) e_i^*(t) + \delta_i(t) \tag{21}$$

where $\delta_i(t) = d_i(t) - \bar{x}_i^*(t+1) + A_i \bar{x}_i^*(t) + B_i \bar{u}_i^*(t)$.

Remark 7. *In this work, the design based on the minimum disturbance upper limit can ensure robust constraints in the worst-case scenario of interconnected power systems and avoid major accidents [38]–[40]. Compared to the strategies that rely on real-time disturbance estimation [41], [42], our controller has lower online computational complexity when the disturbance upper bound is known, making it suitable for operating conditions with limited computing resources.*

B. Stability Analysis

Lemma 1. *[24] System $\dot{x} = f(x, u)$ is input-to-state, if there exists $\mho \in \mathcal{K}_\infty$, $\gamma \in \mathcal{K}_\infty$ and $L > 0$, then the following inequality holds*

$$\|x(t)\| \leq \mho(\|x(0)\|, k) + L\gamma(\|u\|_\infty)$$

The stability of the power system depends on whether it maintains its rated frequency under disturbances and noises. The following theorem ensures the stability of power systems.

Theorem 1. *Let $d_i(t) = 0$ in (20) and define diagonal positive definite matrices Γ_i and W_i with $\rho > 0$, then the strict passivity of the noise-free system of all subsystems implies the asymptotic stability of the noise-free system of the overall system if*

$$\begin{aligned} & \left([\Gamma_i(t)]_j - \rho\right) \alpha_i(t) \geq \left|\Phi_i^{\max}\right|_j \alpha_i(t) + \left|\Psi_i^{\max}\right|_j \alpha_i(t), \\ & [W_i(t)]_j \alpha_i(t) \leq \alpha_i(t) / \left|\Upsilon_i^{\max}\right|_j \end{aligned} \tag{22}$$

Proof. For the noise-free system, we define the output vector $\tilde{y}_i(t) = C_i x_i(t) + W_i w_i(t)$ and $\tilde{y}_i(t) \in C_i \mathcal{X}_i(t) \oplus W_i \mathcal{W}_i(t)$. Based on [24], the strict passivity of each subsystem leads to $\|x_i(t+1)\|^2_{P_i} - \|x_i(t)\|^2_{P_i} \leq \tilde{y}_i^T(t) w_i(t) - \|x_i(t)\|^2 \Gamma_i(t)$.

Define a Lyapunov function $V_i(x_i(t)) = \|x_i(t)\|^2_{P_i}$. Then, all the above discussions can be summarized as

$$V(x(t+1)) - V(x(t)) \leq \tilde{y}^T(t) w(t) - \|x(t)\| \Gamma(t) \tag{23}$$

To satisfy the asymptotic stability, we have the inequality $\tilde{y}^T(t) w(t) - \|x(t)\| \Gamma(t) < 0$ which can be rewritten as

$$\|x(t)\|^2 \Gamma(t) - C^T W_g C - C^T A_g^T W A_g C \geq \rho \|x(t)\|^2 \tag{24}$$

where W_g is the degree matrix.

Based on the Schur Complement, we can obtain that

$$\left[\begin{array}{cc} \Gamma(t) - C^T W_g C - \rho I_n & C^T A_g^T \\ * & W^{-1} \end{array}\right] \geq 0 \tag{25}$$

To replace the uncertain parameters A_g and W_g with their upper bounds, we construct $A_g^{\max}(t)$ and $W_g^{\max}(t)$. Similarly, we construct $\Phi_g^{\max}(t)$, $\Psi_g^{\max}(t)$ and $\Upsilon_g^{\max}(t)$ based on the definitions of $\Phi = C^T W_g C$, $\Psi = C^T A_g^T$ and $\Upsilon = A_g C$ to replace uncertain parameters in Φ, Ψ and Υ with their upper bounds. By using diagonal dominance [40], (25) can be transformed into (22).

This completes the proof. □

Remark 8. *Note that the resulting inequalities are functions of the uncertain parameters. More conservative inequalities can be obtained by replacing the uncertain parameters with their upper bounds, leading to (22).*

Theorem 2. *The closed-loop system (21) is input-to-state stable with respect to $\delta_i(t)$ if the MPC scheme (19) is executed.*

Proof. For the disturbance-free system, based on system (21) and a Lyapunov function $V_i(e_i^*(t)) = \|e_i^*(t)\|_{P_i}^2$, we have

$$\begin{aligned} \triangle V_i \leq & -(\gamma_i - \epsilon_i)\|e_i^*(t)\|_{P_i}^2 \\ & -\epsilon_i \|e_i^*(t)\|_{P_i}^2 + \|\delta_i(t)\|_{P_i}^2 \\ & + 2\|\delta_i(t)\|_{P_i} \left\|A_{K_i}^*(t)e_i^*(t)\right\|_{P_i} \end{aligned} \tag{26}$$

where $\triangle V_i = V_i\left(A_{K_i}^*(t)e_i^*(t) + \delta_i(t)\right) - V_i\left(e_i^*(t)\right)$ and $0 < \epsilon_i < \gamma_i$.

To ensure $\triangle V_i < 0$, it can be obtained that

$$\epsilon_i \|e_i^*(t)\|_{P_i}^2 \geq \|\delta_i(t)\|_{P_i}^2 + 2\|\delta_i(t)\|_{P_i} \left\|A_{K_i}^*(t)e_i^*(t)\right\|_{P_i} \tag{27}$$

Furthermore, by considering $\left\|A_{K_i}^*(t)e_i^*(t)\right\|_{P_i} < \|e_i^*(t)\|_{P_i}$, we can deduce that

$$\epsilon_i \|e_i^*(t)\|^2 - \lambda_{\max}(P_i)\delta_{\max}^2 - 2\lambda_{\max}(P_i)\delta_{\max}\|e_i^*(t)\| \geq 0 \tag{28}$$

where $\lambda_{\max}(P_i)$ is the maximum eigenvalue of P_i, $\delta_{\max}$ is the maximum norm of $\delta_i(t)$.

According to the calculation of the roots of the function on left side in (28), we have

$$\|e_i^*(t)\| \geq \upsilon_i \delta_{i\max}/\epsilon_i \tag{29}$$

where $\upsilon_i = \lambda_{\max}(P_i) + \sqrt{\lambda_{\max}^2(P_i) + \epsilon_i\lambda_{\max}(P_i)}$.

Since $\triangle V_i < 0$, the input-to-state stability of (21) can be derived based on **Lemma 1**.

This completes the proof. □

C. Learning-based tube MPC algorithm

Based on the learning and adaptation stages of the proposed scheme, a robust constraint condition is derived that can restrict the state error between the actual state and the nominal state, thereby ensuring the stability of the actual power system. In addition, due to its ability to learn disturbances sets, the algorithm can effectively deal with unknown disturbances, which makes its applicability not be limited to a single system or structure. The proposed algorithm can be summarized as

Algorithm 1: Learning-based tube MPC algorithm

```
Online part: Solve the optimization control (19).
while Number of iterations not reached do
    Set t = 0 and initial states x̄_i(0) = x_i(0);
    // Ensure e_i(0) = 0 to achieve
       effective feedback control.
    for t to t + 1 do
        Solve the optimization control problem (19)
         based on the constraints (16) and (18).
    end
    // Identify set W_i(t) to obtain
       optimal nominal tracking by
       learning boundary conditions
```

$$-a_{ij}^{\min}(t) = \min e_{ij}^T(t)\theta_i,\ a_{ij}^{\max}(t) = \max e_{ij}^T(t)\theta_i$$
$$\text{s.t.} \begin{bmatrix} F_i \\ \Omega_i(t-1) \end{bmatrix}\theta_i \leq \begin{bmatrix} f_i(t-1) \\ \omega_i(t-1) \end{bmatrix}.$$

```
    for i = 1 to 4 do
        Update the actual state u_i(t) through control
         law u_i(t) = ū_i(t) + K_i(x_i(t) − x̄_i(t)).
    end
    // Obtain the error dynamics (21)
       and ensure the stability of its
       by executing (19).
    Set t = t + 1;
end
```

Remark 9. *By using the tail sequence [43], [44], we can deduce that the proposed learning-based tube MPC scheme (19) is recursively feasible.*

IV. Case Study

The system performance of the learning-based tube MPC method and other control strategies in interconnected power systems with four HESS units are compared and discussed on an improved New England IEEE 10-generator 39-bus system, as shown in Fig. 4.

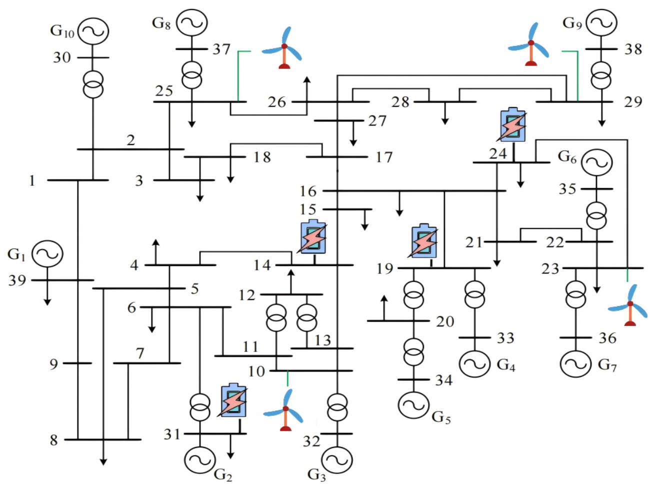

Fig. 4. An improved IEEE 39-bus system with wind power and HESS units.

The hybrid energy storage system primarily serves to smoothing power fluctuations, minimizing system oscillations, and lessening the disparity between peak and valley levels in the power curve. As is well known, batteries have high energy density but low power density and slow dynamic response, while supercapacitors have high power density, fast response speed, and long service life but low energy density. The hybrid energy storage system composed of the two can complement each other's advantages, reduce the rated capacity of the battery and extend its life [33]. Based on the active parallel scheme, a HESS that integrating batteries and supercapacitors is chosen to meet the demands for high power density supply, and its structure is shown in Fig. 5.

Table II shows the power system parameters. To optimize the performance of the considered system, HESS parameters composed of batteries and supercapacitors are set and adjusted according to (30).

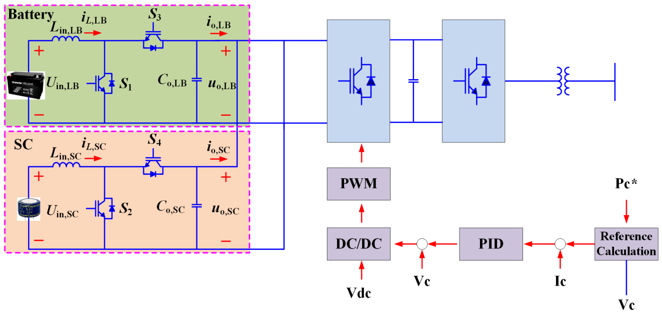

Fig. 5. Structure diagram of hybrid energy storage system.

TABLE II
POWER SYSTEM PARAMETERS

Area-i	T_{mi}	T_{di}	T_{gi}	T_{Ri}	β_i	D_i
Area-1	18	0.3	0.08	2.3	0.42	2
Area-2	20	0.35	0.075	2.4	0.42	1
Area-3	22	0.35	0.075	2.45	0.42	1
Area-4	25	0.355	0.07	2.5	0.42	1

$$\begin{aligned}\frac{di_{Bc}}{dt} &= -\frac{R_B}{L_{Bat}}i_{Bc} - (1-q_1)\frac{U_{dc}}{L_{SC}} + \frac{U_{Bat}}{L_{SC}} \\ \frac{di_{SC}}{dt} &= -\frac{R_S}{L_{SC}}i_{SC} - q_{23}\frac{U_{dc}}{L_{SC}} + \frac{U_{SC}}{L_{SC}} \\ \frac{dU_{dc}}{dt} &= (1-q_1)\frac{i_{Bc}}{C} + q_{23}\frac{i_{SC}}{C} - \frac{i_0}{C}\end{aligned} \tag{30}$$

where L_{SC} and L_{Bat} represent the high-frequency inductors in supercapacitors and batteries, respectively. U_{Sc} and U_{Bat} represent the voltage of the supercapacitors and the batteries, respectively. i_{Bc} is the inductor current and i_{SC} is the current of L_{SC}. V_{Bat} is the capacities of batteries and V_{SC} is the capacities of supercapacitors. U_{dc} is the DC bus voltage. The PWM signal obtained by IGBT K1 operating in boost state is described as q_1, and q_{23} describes the control input of the DC/DC converter.

In this work, the power systems disturbed by the load increment of 0.25 p.u. (750 kW). Moreover, the noises of the equipment is considered to increase the uncertainty of external interference in the interconnected power system, and tube MPC controllers are designed for Area-i to obtain online boundary information of system states based on LFC model of considered systems. In addition, PID, H∞ [34], and max-min [35] control strategies are selected to participate in the frequency deviation simulation of each area for case discussion with the proposed strategy.

A. Case 1: The system response of each control area in different control methods.

In multi-area power systems, the excessive overshoot can result in significant frequency fluctuations, unstable system behavior, and prolonged deviations from the desired frequency. Conversely, the undershoot may cause the slow frequency adjustments, impairing the system's ability to swiftly adapt to load variations, which can also lead to long-term frequency deviations from the target. Therefore, it is crucial to address the issues of overshoot and undershoot.

TABLE III
PERFORMANCE COMPARISON OF EACH AREA UNDER DIFFERENT CONTROL STRATEGIES

Responses	Index$\times(10^{-3})$	H∞	Max-min	Proposed method
Δf_1	Overshoot	0.9751	0.6648	$\mathbf{0.2218}$
	Undershoot	-6.1517	-3.2649	$\mathbf{-1.3516}$
Δf_2	Overshoot	1.0371	0.7741	$\mathbf{0.2016}$
	Undershoot	-5.8534	-2.9413	$\mathbf{-1.0018}$
Δf_3	Overshoot	0.8014	0.5535	$\mathbf{0.1664}$
	Undershoot	-5.7174	-2.2287	$\mathbf{-1.4428}$
Δf_4	Overshoot	0.8757	0.4205	$\mathbf{0.2698}$
	Undershoot	-4.9576	-2.5272	$\mathbf{-1.2487}$

Effective methods for regulating overshoot and undershoot are essential to ensure the safety and stability of multi-area power systems, keeping system voltage and frequency within safe limits. The comparison of overshoot and undershoot of the studied system based on the proposed strategy and other control strategies is provided in Table III. We can see that the learning-based tube MPC method outperforms other controllers, demonstrating excellent performance.

The comparison of the system response simulation results of the four control methods is shown in Fig. 6, which mainly compares the frequency deviation of Area-i. Comparative experiments revealed that when HESS is involved in frequency modulation under identical load disturbances, method with an external PID controller fails to promptly address load changes. Conversely, implementing robust external controllers for the HESS in frequency modulation strategies results in reduced frequency fluctuations. Our strategy can dynamically learn and adapt to robust disturbance invariant sets, allowing it to swiftly and effectively manage load changes. This capability ensures that system frequency deviations remain minimal, thereby achieving system stabilization.

Remark 10. *The proposed strategy minimizes conservatism while improving flexibility, which is suitable for multi-area power systems with the rich data and complex disturbance characteristics. In addition, studying disturbance invariant sets that can accommodate more disturbances such as parameter uncertainty is a future work.*

B. Case 2: The impact of parameter changes in the proposed strategy on regional control performance.

In this work, $\mathcal{Z}_i$, K_i, $\bar{\mathcal{X}}_i$ and $\bar{\mathcal{U}}_i$ are calculated at each moment based on set $\mathcal{W}_i(t)$ which is a function of $a_{ij}^{\min}$ and

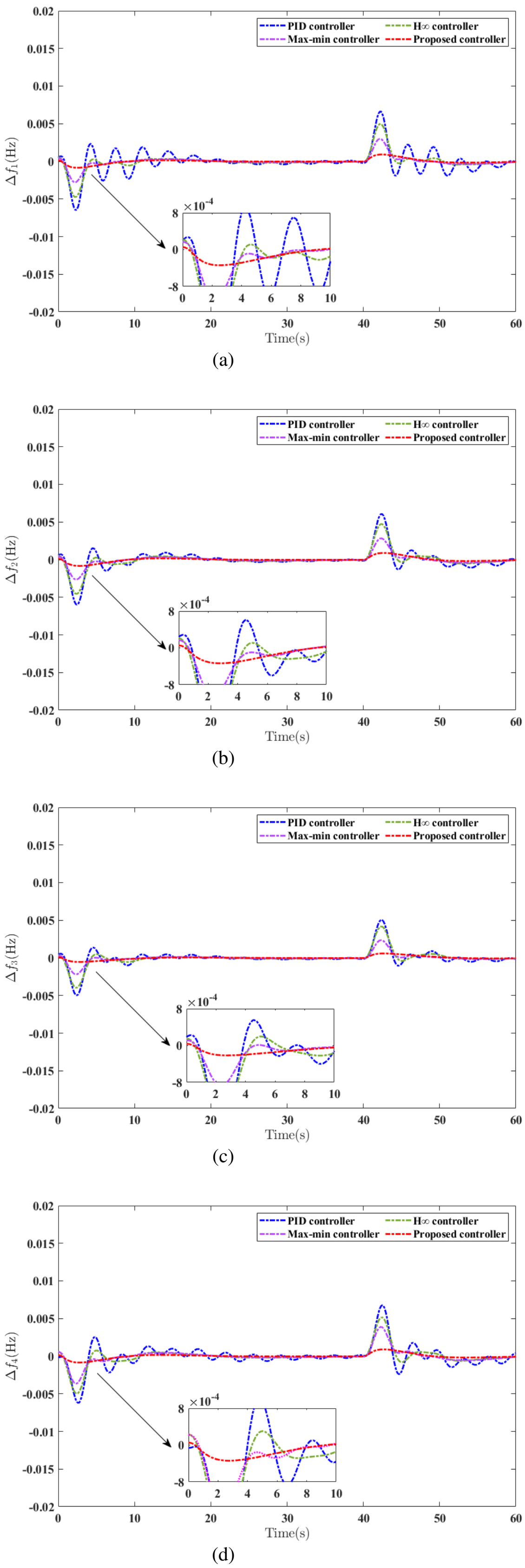

Fig. 6. The system response Δf_i with different control methods in Area-i. (a) Δf_1. (b) Δf_2. (c) Δf_3. (d) Δf_4.

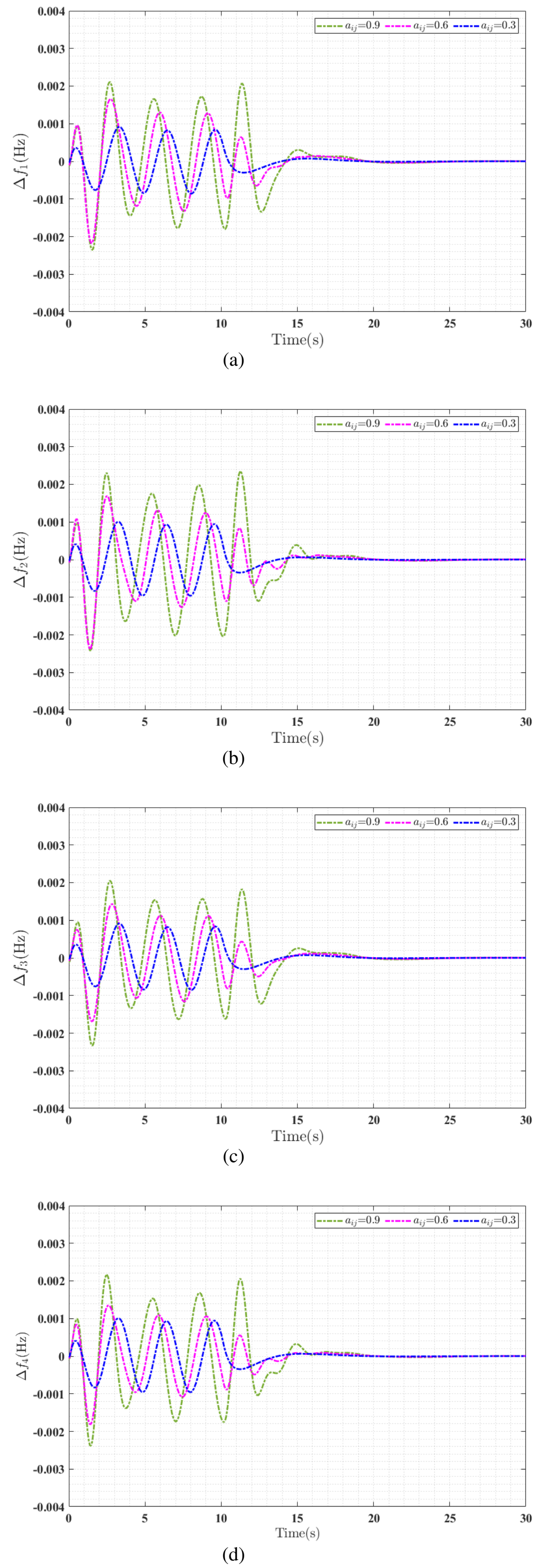

Fig. 7. Δf_i with different updated parameters in Area-i. (a) Δf_1. (b) Δf_2. (c) Δf_3. (d) Δf_4.

$a_{ij}^{\max}$ at time t. Assume that the parameters a_{12} and a_{43} are initially located between 0 and 2, while all other parameters are initially located between 0 and 1.

The frequency response of Area-i with different parameters of the proposed strategy are shown in Fig. 7. Obviously, the differences in updating parameters of the proposed strategy lead to differences in the convergence speed and fluctuation amplitude of frequency deviation in various areas of the power systems. This indicates that the efficiency of learning invariant sets during learning stage is influenced by updating parameters, which in turn changes the optimal output during the adaptation stage. Benefiting from the robustness of the tube control strategy, the proposed strategy can maintain excellent stability when updating the learning parameters.

Remark 11. *The size of the invariant set is directly related to control performance. Larger invariant sets have stronger tolerance for disturbances and higher robustness, but this means that the optimization space of the nominal system is compressed, which may sacrifice response speed and tracking accuracy. Correspondingly, small-sized invariant sets are sensitive to disturbances and have reduced robustness, but they allow the nominal system to optimize under tighter constraints, potentially achieving better dynamic performance [45]. Therefore, it is crucial to design and optimize tube size based on actual operating conditions to balance system performance and stability, which is also the motivation for introducing learning mechanisms into the proposed strategy.*

V. Conclusion

We proposed a learning-based tube MPC strategy for multi-area interconnected power systems with wind power and HESS. This strategy mitigated the negative impact of disturbance and noise in the considered power systems by identifying the uncertainty invariant sets of the online data coupling strength during the learning stage and handling the corresponding optimal MPC problem during the adaptation stage. To validate the correctness of the control method, a reliability criterion was developed to prove the applicability of the learning-based tube MPC strategy. The benefits of our strategy for optimizing frequency control were demonstrated by comparing the applications of various strategies within four-area power systems. While both disturbance and noise interference factors have been taken into consideration, there are still factors such as parameter uncertainty that may affect the stability of the system. Therefore, the focus of future work will mainly be on researching control strategies that can handle multiple composite disturbances to achieve better load frequency control performance in power systems.

References

[1] M. Zhang, S. Dong, and P. Shi, "Distributed observer-based event-triggered load frequency control of multiarea power systems under cyber attacks," *IEEE Transactions on Automation Science and Engineering*, vol. 20, no. 4, pp. 2435–2444, 2019.

[2] Q. Pang, V. Trovato, and A. D. Paola, "Market-based operation of interconnectors in a multi-area power network with meshed topology," *IEEE Transactions on Energy Markets, Policy and Regulation*, vol. 2, no. 1, pp. 79–91, 2024.

[3] R. K. Subroto, K. L. Lian, and C. C. Chu, "A fast frequency control based on model predictive control taking into account of optimal allocation of power from the energy storage system," *IEEE Transactions on Power Delivery*, vol. 36, no. 4, pp. 2467–2478, 2021.

[4] M. Ma, X. Liu, and C. Zhang, "LFC for multi-area interconnected power system concerning wind turbines based on DMPC," *IET Generation, Transmission & Distribution*, vol. 11, no. 10, pp. 2689–2696, 2017.

[5] M. Ma, C. Zhang, and X. Liu, "Distributed model predictive load frequency control of the multi-area power system after deregulation," *IEEE Transactions on Industrial Electronics*, vol. 64, no. 6, pp. 5129–5139, 2017.

[6] D. K. Panda, S. Das, and S. Townley, "Toward a more renewable energy-based lfc under random packet transmissions and delays with stochastic generation and demand," *IEEE Transactions on Automation Science and Engineering*, vol. 19, no. 2, pp. 1217–1232, 2022.

[7] Z. Cheng, X. Bu, and L. Jiaqi, "Indirect–direct secure load frequency control against false data injection attacks," *IEEE Transactions on Industrial Informatics*, vol. 20, no. 3, pp. 4850–4862, 2024.

[8] Y. Shi, C. Liu, and Y. Wang, "Asymptotically stable filter for mvu estimation of states and homologous unknown inputs in heterogeneous multiagent systems," *IEEE Transactions on Automation Science and Engineering*, vol. 19, no. 2, pp. 884–894, 2022.

[9] B. Srikanth, D. Rajeeb, and M. Saad, "Linear quadratic differential games based MIMO-PID design for load frequency control of a 2-area interconnected power system: An iterative LMI approach," *IFAC PapersOnline*, vol. 56, no. 2, pp. 348–353, 2023.

[10] F. Liu, Y. Li, and Y. Cao, "A two-layer active disturbance rejection controller design for load frequency control of interconnected power system," *IEEE Transactions on Power Systems*, vol. 31, no. 4, pp. 3320–3321, 2016.

[11] X. Liu, X. Kong, and K. Y. Lee, "Distributed model predictive control for load frequency control with dynamic fuzzy valve position modelling for hydro-thermal power system," *IET Control Theory & Applications*, vol. 10, no. 14, pp. 1653–1664, 2016.

[12] Y. Li, X. Li, and J. Cheng, "Reliable quantized sampled-data LFC for semi-Markov jump interconnected multi-area power systems: Dealing with incomplete TRs," *International Journal of Robust and Nonlinear Control*, vol. 34, no. 5, pp. 3241–3285, 2024.

[13] Z. Cheng, X. Bu, and J. Liang, "Indirect–direct secure load frequency control against false data injection attacks," *IEEE Transactions on Industrial Informatics*, vol. 20, no. 3, pp. 4850–4862, 2024.

[14] H. Wang and Z. S. Li, "Multi-area load frequency control in power system integrated with wind farms using fuzzy generalized predictive control method," *IEEE Transactions on Reliability*, vol. 72, no. 2, pp. 737–747, 2023.

[15] M. Zhang, S. Dong, and Z. Wu, "Reliable event-triggered load frequency control of uncertain multiarea power systems with actuator failures," *IEEE Transactions on Automation Science and Engineering*, vol. 20, no. 4, pp. 2516–2526, 2023.

[16] H. Yang, B. Li, Z. Zuo, and Z. Hai, "Tube-based MPC for LPV systems with external disturbances using interval predictors," *IEEE Transactions on Industrial Informatics*, vol. 20, no. 3, pp. 3060–3069, 2024.

[17] Y. Yang, G. Y. Hen, and N. Richard, "A robust model predictive control-based scheduling approach for electric vehicle charging with photovoltaic systems," *IEEE Systems Journal*, vol. 17, no. 1, pp. 111–121, 2023.

[18] J. Wu and K. Yu, "Adaptive tube model predictive control for manipulating micro- and nanoparticles in fluid suspensions under global external fields," *IEEE Transactions on Automation Science and Engineering*, vol. 20, no. 3, pp. 1838–1850, 2023.

[19] M. Shiroei, M. R. Toulabi, and A. M. Ranjbar, "Robust multivariable predictive based load frequency control considering generation rate constraint," *International Journal of Electrical Power and Energy Systems*, vol. 46, pp. 405–413, 2013.

[20] I. Kiaei, M. Rostami, and S. Lotfifard, "Robust decentralized control of synchronous generators for improving transient stability of multimachine power grids," *IEEE Systems Journal*, vol. 15, no. 3, pp. 3470–3479, 2021.

[21] J. Cao, C. Yin, and R. Wang, "Dynamic thermal management of proton exchange membrane fuel cell vehicle system using the tube-based model predictive control," *International Journal of Hydrogen Energy*, vol. 70, pp. 493–509, 2024.

[22] A. Oshnoei, M. Kheradmandi, S. M. Muyeen, and N. Hatziargyriou, "Disturbance observer and tube-based model predictive controlled electric vehicles for frequency regulation of an isolated power grid," *IEEE Transactions on Smart Grid*, vol. 12, no. 5, pp. 4351–4362, 2021.

[23] X. Liu, C. Wang, and X. Kong, “Tube-based distributed MPC for load frequency control of power system with high wind power penetration,” *IEEE Transactions on Power Systems*, vol. 19, no. 1, pp. 1–12, 2023.
[24] X. Liu, L. Feng, and X. Kong, “Tube-based stochastic model predictive control with application to wind energy conversion system,” *IEEE Transactions on Control Systems Technology*, vol. 31, no. 5, pp. 2173–2187, 2023.
[25] P. Fan, J. Yang, and S. Ke, “Load frequency control strategy for islanded multimicrogrids with V2G dependent on learning-based model predictive control,” *IET Generation, Transmission & Distribution*, vol. 17, no. 21, pp. 4763–4780, 2023.
[26] R. Wang, H. Li, and B. Liang, “Policy learning for nonlinear model predictive control with application to USVs,” *IEEE Transactions on Industrial Electronics*, vol. 71, no. 4, pp. 4089–4097, 2024.
[27] X. Tang, Y. Li, and M. Yang, “Adaptive event-triggered model predictive load frequency control for power systems,” *IEEE Transactions on Power Systems*, vol. 38, no. 5, pp. 4003–4014, 2023.
[28] Q. Jiang and H. Hong, “Wavelet-based capacity configuration and coordinated control of hybrid energy storage system for smoothing out wind power fluctuations,” *IEEE Transactions on Power Systems*, vol. 28, no. 2, pp. 1363–1372, 2013.
[29] Y. Liu and M. Peng, “Research on peak load shifting for hybrid energy system with wind power and energy storage based on situation awareness,” *Journal of Energy Storage*, vol. 82, pp. 1–13, 2024.
[30] K. B. Pradyumna and P. Monalisa, “Supervisory power management scheme of a laboratory scale wind-PV based LVDC microgrid integrated with hybrid energy storage system,” *IEEE Transactions on Industry Applications*, vol. 60, no. 3, pp. 4723–4735, 2024.
[31] Z. Liu, J. Guo, and Y. Li, “Multi-scenario analysis and collaborative optimization of a novel distributed energy system coupled with hybrid energy storage for a nearly zero-energy community,” *Journal of Energy Storage*, vol. 41, p. 102992, 2021.
[32] L. Yin and Y. Li, “Hybrid multi-agent emotional deep Q network for generation control of multi-area integrated energy systems,” *Applied energy*, vol. 324, no. 15, pp. 1–33, 2022.
[33] Q. Zhang, F. Ju, and S. Zhang, “Power management for hybrid energy storage system of electric vehicles considering inaccurate terrain information,” *IEEE Transactions on Automation Science and Engineering*, vol. 14, no. 2, pp. 608–618, 2017.
[34] W. Yan, L. Sheng, D. Xu, W. Yang, and Q. Liu, “H ∞ robust load frequency control for multi-area interconnected power system with hybrid energy storage system,” *Applied Sciences*, vol. 8, no. 10, p. 1748, 2018.
[35] A. Oshnoei, M. Kheradmandi, and S. M. Muyeen, “Robust control scheme for distributed battery energy storage systems in load frequency control,” *IEEE Transactions on Power Systems*, vol. 35, no. 6, pp. 4781–4791, 2020.
[36] Z. An, X. Liu, G. Song, G. Xiao, and P. Wang, “Tube-based mpc strategy for load frequency control of multi-area interconnected power system with HESS,” *Journal of Energy Storage*, vol. 99, pp. 1–17, 2024.
[37] H. J. Waarde, M. K. Camlibel, and M. Mehran, “From noisy data to feedback controllers: Nonconservative design via a matrix S-lemma,” *IEEE Transactions on Automatic Control*, vol. 67, no. 1, pp. 162–175, 2022.
[38] F. Giulio, R. Michela, and S. Roberto, “A fully distributed robust MPC approach for frequency and voltage regulation in smart grids with active and reactive power constraints,” *IEEE Transactions on Systems, Man, and Cybernetics: Systems*, vol. 54, no. 11, pp. 6657–6669, 2024.
[39] Q. Li, Y. Shi, and Y. Jiang, “A distributionally robust model predictive control for static and dynamic uncertainties in smart grids,” *IEEE Transactions on Smart Grid*, vol. 15, no. 5, pp. 4890–4902, 2024.
[40] Y. Zhang, G. Li, and A. A. Mustafa, “Robust learning-based model predictive control for wave energy converters,” *IEEE Transactions on Sustainable Energy*, vol. 15, no. 3, pp. 1957–1967, 2024.
[41] C. Li, C. Sun, Z. Chen, and Y. Zhang, “Broad learning system using rectified adaptive moment estimation for harmonic detection and analysis,” *IEEE Transactions on Industrial Electronics*, vol. 71, no. 3, pp. 2873–2882, 2024.
[42] Z. Ye and K. W. E. Cheng, “Design and validation of a multioutput wireless power transfer system using MPC controller,” *IEEE Transactions on Power Electronics*, vol. 39, no. 12, pp. 16 065–16 077, 2024.
[43] L. Yang, A. Ma, and D. Li, “Input-mapping based data-driven model predictive control for unknown linear systems with bounded disturbances,” *Automatica*, vol. 153, p. 111056, 2023.
[44] R. Heydari and M. Farrokhi, “Robust tube-based model predictive control of LPV systems subject to adjustable additive disturbance set,” *Automatica*, vol. 129, p. 109672, 2021.
[45] H. Shen, W. Zhao, J. Cao, J. H. Park, and J. Wang, “Predefined-time event-triggered tracking control for nonlinear servo systems: A fuzzy weight-based reinforcement learning scheme,” *IEEE Transactions on Fuzzy Systems*, vol. 32, no. 8, pp. 4557–4569, 2024.